CHAPTER 4
A STUDY OF PHOTOCATALYTIC ACTIVITY OF GRAPHENE–TITANIUM DIOXIDE (GR–TiO_2) PHOTOCATALYST

4.1 Introduction

Titanium dioxide (TiO_2) photocatalyst is the most commonly used material for environmental remediation because of its high chemical stability, non–toxicity, low cost and strong photocatalytic activity. However, it has been reported that the photocatalytic activity of TiO_2 is limited because of its large band gap (3.2 eV) and low adsorption property (Wellia et al., 2011). Adsorption can be increased by increasing the surface area of the catalyst, and it has been reported that the photocatalytic activity can be enhanced by adsorption because adsorbed organic pollutants are further degraded on the surface of the catalyst (Bhatkhande et al. 2001).Therefore, an increase in the adsorption capacity should improve the photocatalytic activity.

Several materials have been used to synthesize co–adsorbents for TiO_2 such as clays (Kibanova et al., 2012), zeolites (Ichiura et al., 2003 and Wang et al., 2011b) and carbon–based adsorbent materials (Leary and Westwood, 2011) in order to improve the photocatalytic activity of TiO_2. Activated carbon (AC) (Fu et al., 2004 and Miyawaki et al., 2011), carbon nanotubes (CNT) (Chen et al., 2012 and Cong et al., 2011) and graphene (GR) (Hou et al., 2012 and Wang et al., 2012) have been widely used as co–adsorbent materials because of their large surface area. Recently, graphene has been used in many applications such as energy–storage, nanoelectronic devices and catalysis, owing to its two-dimensional sp^2 bonding network of carbon atoms, which gives it outstanding electrical, thermal, mechanical, and optical properties (Li et al., 2011; Qianqian et al., 2011 and Lv et al., 2012).

Graphene–TiO_2 (GR–TiO_2) heterogeneous photocatalysis has received much attention for the degradation of organic pollutants. So far, commercial grade titanium dioxide, Degussa P25, was generally used as the TiO_2 source. The photocatalytic activities of pure P25, P25–graphene, and P25–carbon nanotubes have been examined. The results illustrate that P25–graphene shows higher photocatalytic activity than P25–carbon nanotube catalyst

under UV and visible light irradiation (Zhang et al., 2010b). The enhanced photocatalytic activity of semiconductor photocatalysts by adding graphene has received much attention in many applications such as hydrogen production (Zhang et al., 2012) and degradation of organic pollutants (Zhao et al., 2012).

Oxygen-containing functional groups on the surface of graphene oxide such as epoxy, alkoxy and carboxyl act as a good support material to produce GR–TiO_2 (Jiang et al., 2011 and Wang et al., 2011c). Hydrothermal treatment is a popular technique to prepare GR–TiO_2 composites, the homogeneous GR–TiO_2 suspension is transferred to autoclave and maintain at 120–180 °C for 2–24 h (Zhang et. al., 2010a; Zhang et al., 2010b and Cheng et al., 2012). The UV-assisted photocatalytic reduction of graphene oxide, which has been reported as a new reduction technique for preparation GR–TiO_2 photocatalyst, exhibits well-separated GR–TiO_2 composite sheet (Williams et al., 2008). The electronic conductivity of graphene by its π–π conjugation structure enhances photocatalytic activity by suppression charge recombination of electron–hole pairs. It has been reported that the extendable photoexcitation under visible light irradiation resulting in the formation of Ti–O–C bonds (Nguyen-Phan et al., 2011). It was noted that excessive graphene content in TiO_2 leads to decrease in photodegradation efficiency because of light obstruction (Wang et al., 2011c). Thus, the optimal graphene content in TiO_2 needs to be investigated and controlled to achieve an adequate photocatalytic activity of GR–TiO_2.

In earlier reports, the traditional sol-gel method was widely used for TiO_2 synthesis. However, this method requires an acidic or baseic catalyst in order to drive hydrolysis and poly-condensation processes. The TiO_2 nanoparticles in acid or base solution are then obtained after calcination at high temperature. Therefore, the acid or base nature of TiO_2 sol and high temperature calcination limit its application, including the choice of substrates (Liu et al., 2008a and Sasirekha et al., 2009). Use of peroxo titanic acid (PTA) is an alternative method for synthesis of pure anatase TiO_2 under neutral pH and low temperature conditions. It was also reported as an environmental friendly method for synthesis of TiO_2 because peroxotitanium complex molecules can be converted into TiO_2 nanoparticles at relatively low temperature (100 °C) (Seok et al., 2010). Previously, our

group has reported the synthesis of amine functionalized SiO_2/TiO_2 photocatalytic films prepared from refluxed PTA solution at 100 °C for 10 h. The results show that the adsorption capability of the photocatalyst plays an important role in VOC degradation (Boonamnuayvitaya and Photong, 2009). In this work, refluxed PTA solution at 100 °C for 10 h was applied as a starting material for TiO_2 nanoparticles to synthesize GR–TiO_2 composite. Graphene oxide–TiO_2 was reduced to graphene–TiO_2 using UV-assisted photocatalytic reduction without heating. The photocatalytic activity of prepared GR–TiO_2 (PTA) catalysts was examined by evaluating the degradation of MB aqueous solution under UV and visible light irradiation.

4.2 Results and discussion

4.2.1 Physicochemical properties of catalysts

Figure 4.1 shows the X-ray diffraction (XRD) patterns of TiO_2 (PTA refluxed at 100 °C for 2 h), TiO_2 (PTA refluxed at 100 °C for 10 h) and GR–TiO_2 (PTA) composites, there are five distinctive TiO_2 peaks at 25.3°, 37.9°, 48.0°, 54.6°, and 62.8° which correspond to anatase phase (JCPDS 21–1272). It is clear from Figure 4.1 that TiO_2 synthesized via PTA as a precursor demonstrates exclusively the anatase phase. The crystal sizes of TiO_2 (PTA refluxed at 100 °C for 2) and TiO_2 (PTA refluxed at 100 °C for 10 h) calculated from Scherrer's equation (Table 4.1) are 12.9 and 14.8 nm, respectively. The intensity of the anatase diffraction peak increases with increasing reflux time and the crystal size of anatase phase tends to increase in size because of the enhanced crystallinity. The XRD diffraction patterns of GR–TiO_2 (PTA) composites are similar to those of pure TiO_2. This implies that the crystal structure of TiO_2 (PTA) do not change during the graphene oxide reduction process. However, the increase in crystal size of GR–TiO_2 (PTA) about 15.2 nm may be attributed to the enhanced crystallinity during drying of GR–TiO_2 (PTA) catalyst in a hot air oven at 50 °C for 6 h.

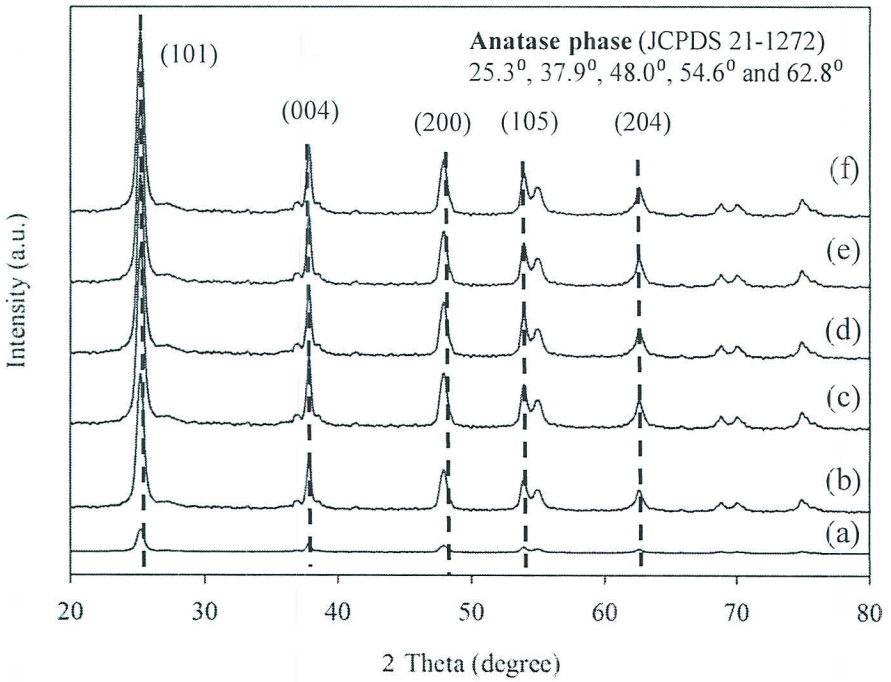

Figure 4.1 XRD diffraction patterns of (a) TiO_2 (PTA refluxed at 100 °C for 2 h), (b) TiO_2 (PTA refluxed at 100 °C for 10 h), (c) GR–TiO_2 (PTA, 1:100), (d) GR–TiO_2 (PTA, 1:50), (e) GR–TiO_2 (PTA, 1:20) and (f) GR–TiO_2 (PTA, 1:10).

Table 4.1 Crystal size of TiO_2 and weight fraction of anatase phase.

Sample	Crystal structure	Anatase phase crystal size (nm)	Rutile phase crystal size (nm)	Weight fraction of anatase phase (%)
TiO_2 (PTA refluxed 2 h)	anatase	12.9	–	100
TiO_2 (PTA refluxed 10 h)	anatase	14.8	–	100
GR–TiO_2 (PTA)	anatase	15.2	–	100

The photocatalytic activities of TiO_2 at various refluxed time were investigated as shown in Figure 4.2. The degradation efficiency of MB in the presence TiO_2 (PTA) increases with increasing refluxed time. It was noted that TiO_2 (PTA refluxed at 100 °C for 10 h) with 40.3% photodegradation seemed to be an optimal refluxed time for the preparation of TiO_2 nanoparticles.

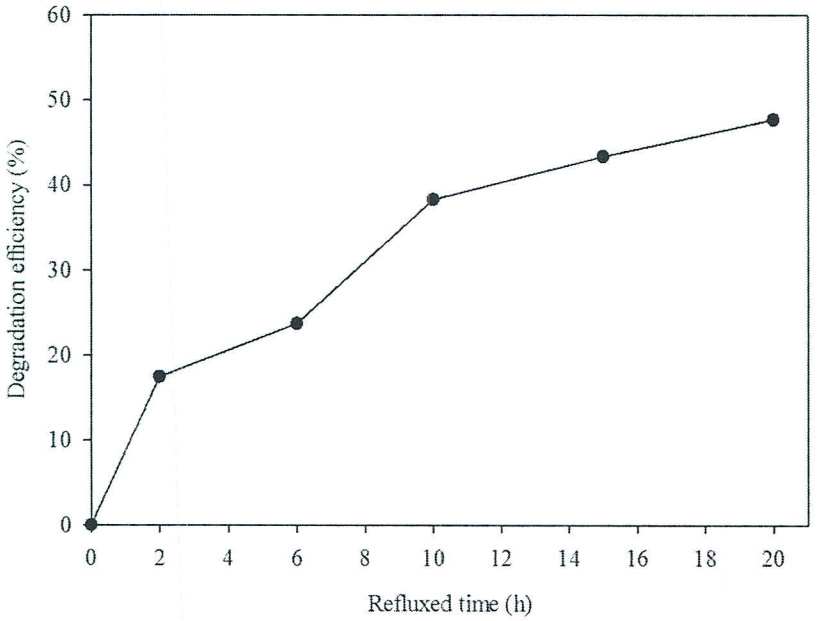

Figure 4.2 Degradation efficiencies of TiO_2 (PTA) at various refluxed time. (MB was used as an indicator.)

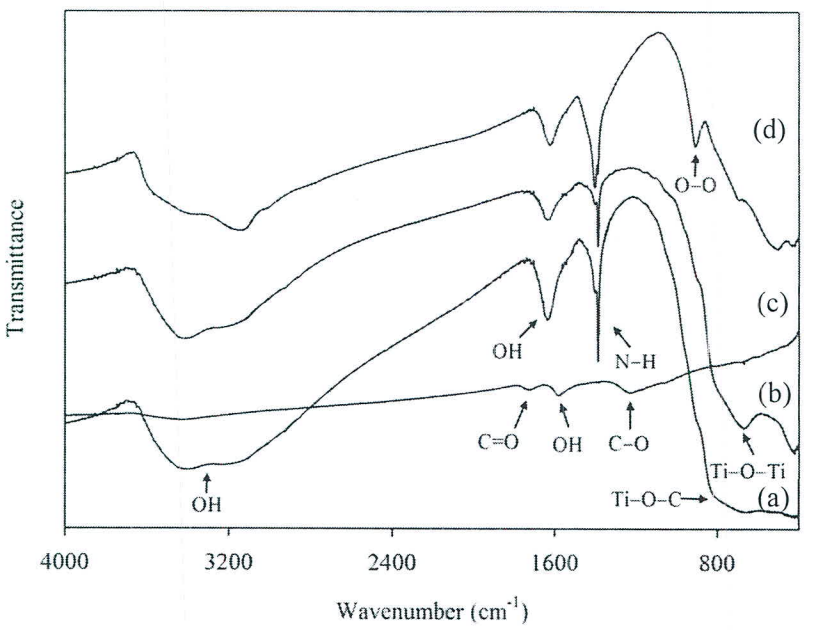

Figure 4.3 FTIR spectra of (a) GR–TiO_2 (PTA) composite, (b) TiO_2 (PTA refluxed at 100 °C for 10 h), (c) graphene oxide powder and (d) PTA powder (non-refluxed).

The functional groups of GR–TiO_2 (PTA) composite, TiO_2 (PTA refluxed at 100 °C for 10 h), graphene oxide powder and PTA (non-refluxed) are presented in Figure 4.3. A broad absorption band at 3000–3600 cm^{-1} and a strong peak at 1632 cm^{-1} can be assigned to the vibration of OH groups of adsorbed water and Ti–OH group. The adsorption peak at around 1400 cm^{-1} is due to the stretching vibration from the N–H bond of the residual NH_4^+. The peak at 900 cm^{-1} can be assigned to the stretching mode of the peroxo group. The intensity of this peak decreased during refluxing because of the decomposition of the peroxo group (Sasirekha et al., 2012 and Ge et al., 2006a). The absorption peak between 400 and 690 cm^{-1} was corresponded to the signal of Ti–O–Ti bond. The absorption peaks at 3420 and 1579 cm^{-1} correspond to the OH group. The peaks at 1723 and 1228 cm^{-1} are assigned as the carbonyl group (C=O) and epoxy group (C–O), respectively.

The FTIR data of GR–TiO_2 (PTA) show different FTIR spectral patterns in comparison with graphene oxide. After the graphene oxide reduction process, the peaks of the carbonyl and epoxy groups disappeared. This implies that the functional groups on graphene oxide were completely reduced to graphene using the UV-assisted photocatalytic reduction method. In addition, it was also observed that the signal of Ti–O–Ti shifted to a higher wavenumber around 790 cm^{-1} because of the combined signal of Ti–O–Ti and Ti–O–C vibration (Ge et al., 2006a and Nguyen-Phan et al., 2011).

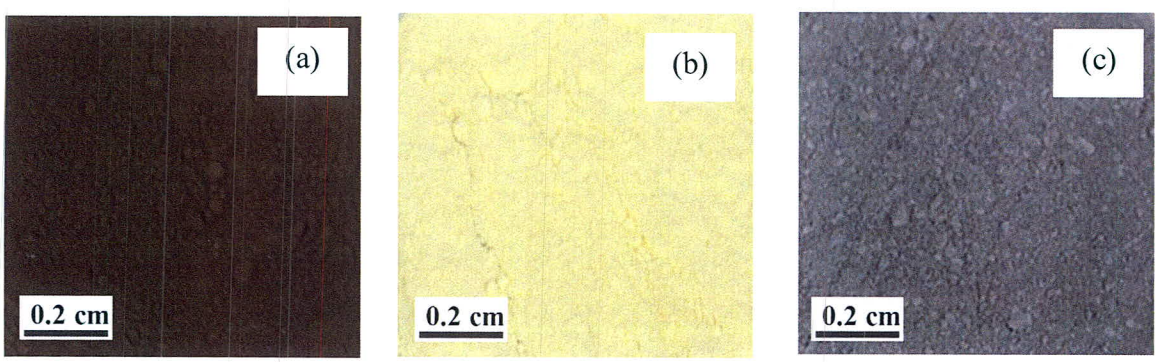

Figure 4.4 Photographs of (a) graphene oxide powder, (b) TiO_2 (PTA refluxed at 100 °C for 10 h) and (c) GR–TiO_2 (PTA) composite. (Canon EOS 450D, EFS 18–55 mm, 10X).

In Figure 4.4, the digital photographs of graphene oxide powder, TiO_2 (PTA refluxed at 100 °C for 10 h), and GR–TiO_2 (PTA) illustrate the color change of the powders. Graphene oxide has a brown color and the TiO_2 (PTA refluxed at 100 °C for 10 h) powder is light-yellow in color because of the remaining peroxo group. After graphene oxide reduction under UV irradiation for 48 h, the color of GR–TiO_2 (PTA) changed to light grey.

The wrinkled two-dimensional structure of graphene oxide can be clearly observed in Figure 4.5. In the case of TiO_2 (PTA refluxed at 100 °C for 10 h), the needle-like or rhombus anatase crystals have an average length of 40–80 nm and diameter of 10–20 nm. The TEM image of GR–TiO_2 (PTA) demonstrates that TiO_2 nanoparticles are successfully loaded onto graphene sheet. However, the crystal size of TiO_2 (PTA) calculated using Scherrer's equation (14.8 nm) was different from the TEM image (80–90 nm in length and 20–22 in diameter) because of the effect of diffraction line width and instrumental broadening (Ge et al., 2006b).

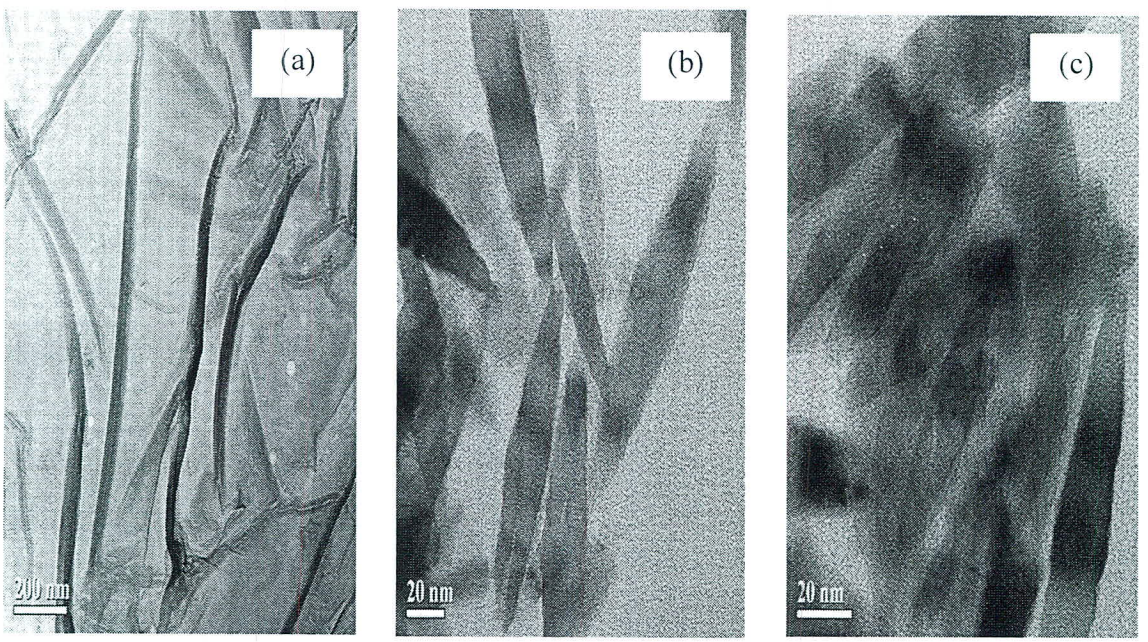

Figure 4.5 TEM images of (a) graphene oxide, (b) TiO_2 (PTA refluxed at 100 °C for 10 h), and (c) GR–TiO_2 (PTA) composite.

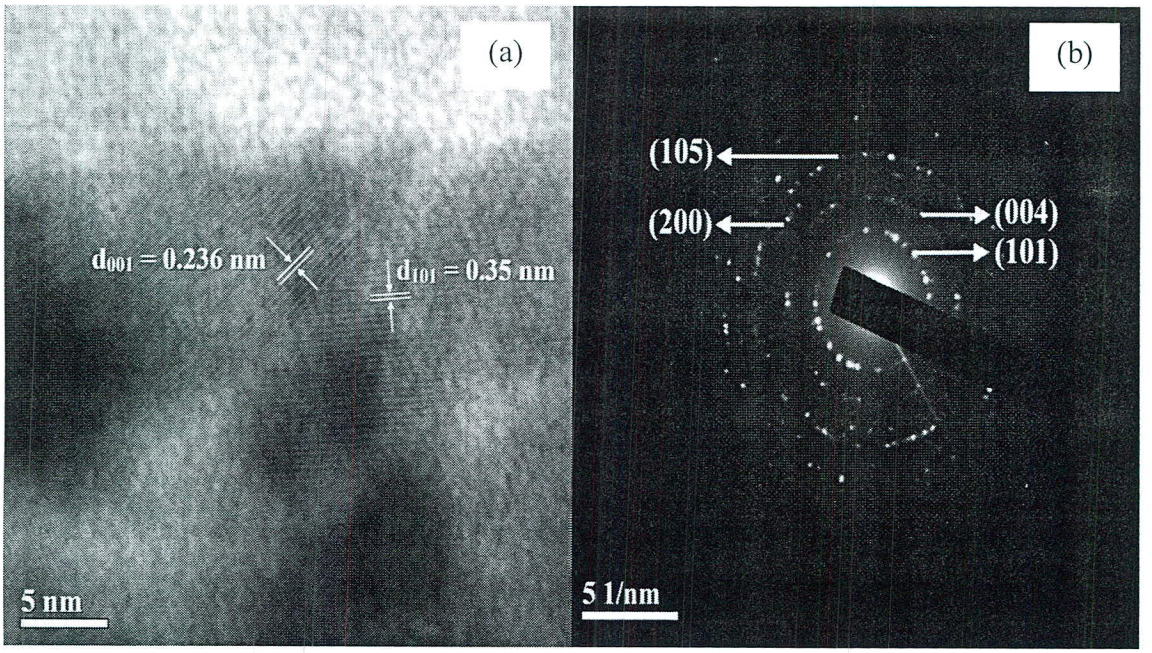

Figure 4.6 (a) High resolution TEM (HRTEM) image and (b) the selected area electron diffraction (SAED) pattern of GR–TiO_2 (PTA) composite.

Figure 4.6 (a) is a high resolution TEM (HRTEM) image of GR–TiO_2 sample. The crystal spacing of 0.236 and 0.35 nm is observed to correspond to the (001) and (101) planes of anatase. Figure 4.6(b) shows the selected area electron diffraction (SAED) pattern of GR–TiO_2 (PTA). The diffraction rings of GR–TiO_2 (PTA), which can be indexed to (101), (004), (200) and (105) crystal planes of anatase TiO_2, are in accordance with the XRD analysis.

The surface texture of the photocatalysts is presented in Table 4.2. The results show that TiO_2 (PTA) and P25 have specific areas of 88.00 and 50.75 $m^2\ g^{-1}$, respectively. The larger surface area of TiO_2 (PTA) was ascribed to the small crystal size. In the case of GR–TiO_2 nanocomposite, the specific surface area seems to increase with increasing weight ratio of graphene oxide. Moreover, the GR–TiO_2 (PTA) catalysts show a significant change in surface area because of the influence of crystal size and the well configuration of TiO_2 (PTA) and graphene.

Table 4.2 Texture characterization of TiO_2 and GR–TiO_2 photocatalysts.

Sample	BET surface ($m^2\ g^{-1}$)	Total pore volume ($cm^3\ g^{-1}$)	Average pore diameter (nm)
P25	50.75	0.47	37.24
TiO_2 (PTA)	88.00	0.36	16.20
GR–TiO_2 (PTA, 1:100)	93.76	0.33	14.07
GR–TiO_2 (PTA, 1:50)	94.13	0.38	16.21
GR–TiO_2 (PTA, 1:20)	102.00	0.20	8.02
GR–wTiO_2 (PTA, 1:10)	105.70	0.31	11.56

The UV-vis absorption spectra of TiO_2 (PTA) and GR–TiO_2 (PTA) catalysts are presented in Figure 4.7. The spectra of GR–TiO_2 (PTA) catalysts show a red shift in the band gap transition with increases in the amount of graphene dopant. The absorption below 400 nm results from the excitation of electrons from the valence band (VB) to the conduction band (CB) of TiO_2. The band gap energy of catalysts can be estimated by the Kubelka–Munk function (Zhang et al., 2010b; Chen et al., 2012 and Ge et al., 2006a).

In Figure 4.8, the estimated band gaps of GR–TiO_2 (PTA) are 3.24, 3.22, 3.20, 3.09, and 2.90, corresponding to TiO_2 (PTA), GR–TiO_2 (PTA, 1:100), GR–TiO_2 (PTA, 1:50), GR–TiO_2 (PTA, 1:20), and GR–TiO_2 (PTA, 1:10), respectively. Analogous results for band gap narrowing of the GR–P25 series were also found (Zhang et al., 2010b and Chen et al., 2012); the decrease in the band gap in the GR–TiO_2 composite was due to the interaction between TiO_2 (PTA) and graphene, which can be clearly observed from the FTIR broad absorption of Ti–O–Ti and Ti–O–C vibrations around 790 cm^{-1}.

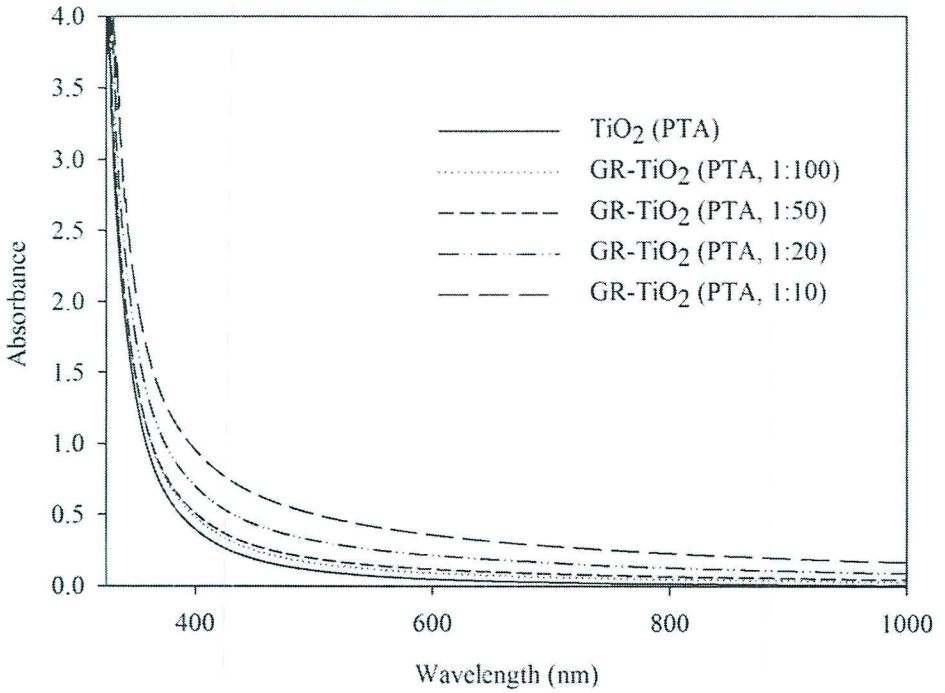

Figure 4.7 UV-vis absorption spectra of photocatalysts.

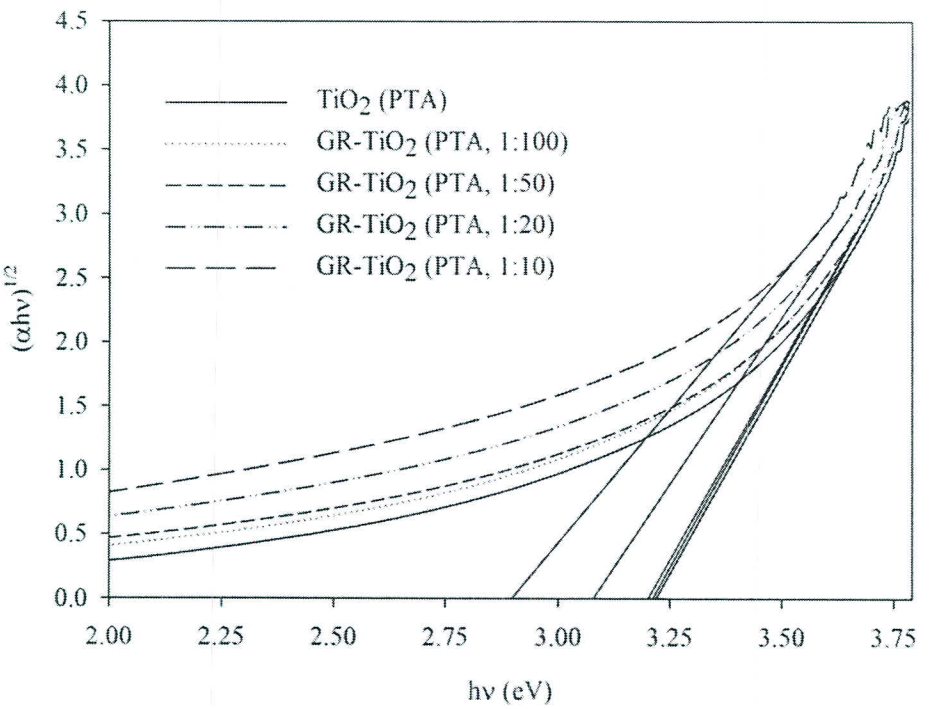

Figure 4.8 Estimated band gaps energy of photocatalysts.

Figure 4.9 shows the photocurrent behavior of TiO_2 (PTA) and GR–TiO_2 (PTA, 1:50) photo catalysts under UV and visible light irradiation. It was observed that photocurrent of all samples show a uniform photoresponse. The photocurrent generations from GR–TiO_2 (PTA) composites are higher than that of pure TiO_2 (PTA). The GR–TiO_2 (PTA, 1:50) photocatalyst, which demonstrated the highest photocurrent generation, yielded the current density of 4.33 and 2.98 μA cm^{-2} under UV and visible light illumination, respectively. The increase in photocurrents can be attributed to the two-dimensional π–π conjugation structure of carbon atoms of graphene resulting in an excellent electrical conduction.

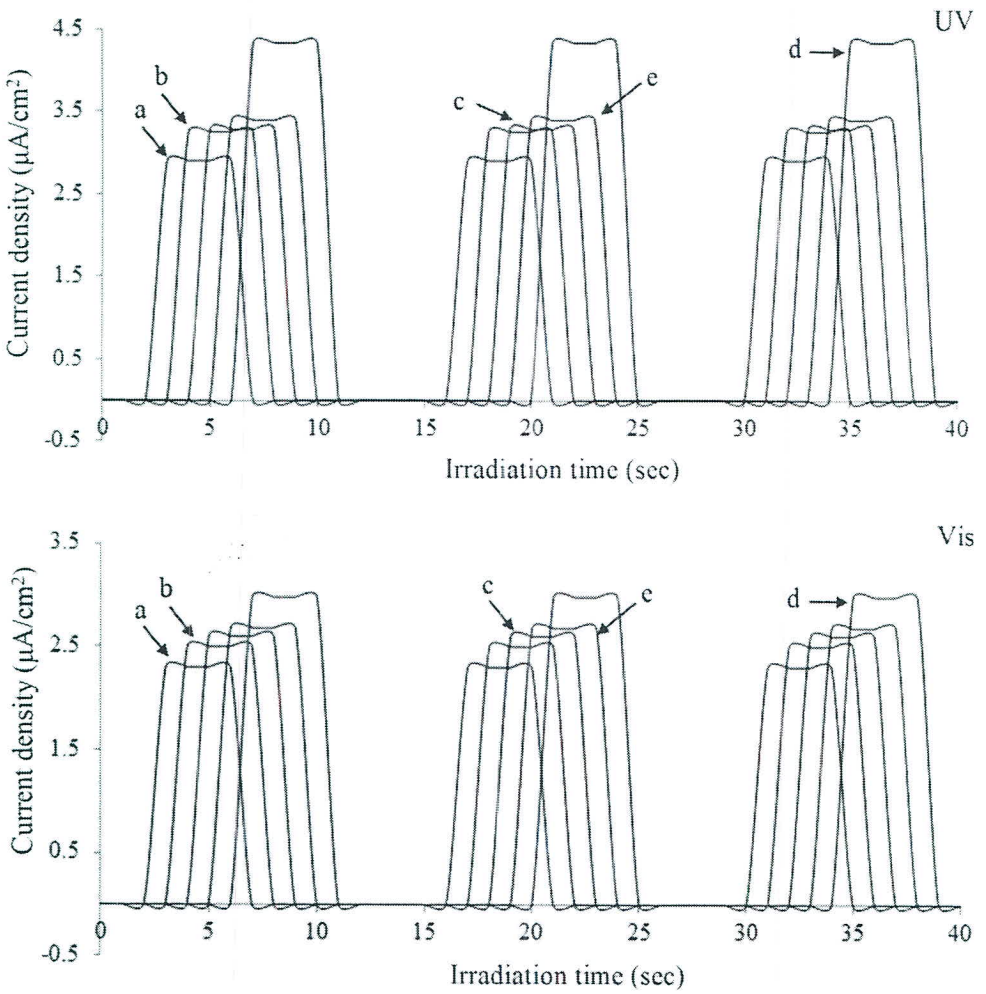

Figure 4.9 Photocurrent behaviors of (a) TiO_2 (PTA), (b) GR–TiO_2 (PTA, 1:10), (c) GR–TiO_2 (PTA, 1:20), (d) GR–TiO_2 (PTA, 1:50) and (e) GR–TiO_2 (PTA, 1:100) photocatalysts under UV and visible light irradiation.

However, the decreasing in photocurrent can be observed on excessive graphene content in GR–TiO_2 (PTA, 1:20 and 1:10) composites. The higher graphene content in GR–TiO_2 (PTA) composite may hinder or scatter the light transmission. Therefore, the photoexcitation of TiO_2 could be decreased because of the light obstruction of graphene (Wang et al., 2011c).

4.2.2 Photocatalytic activities

Figure 4.10 shows the concentration of the MB solution after reaching the adsorption–desorption equilibrium in dark conditions. The equilibrium concentrations of MB in the GR–TiO_2 (PTA) series are lower than that of pure TiO_2 (PTA). This confirms that MB was adsorbed more in the GR–TiO_2 (PTA) series. In addition, GR–TiO_2 (PTA) demonstrates the increased adsorption capacity with increasing weight fraction of graphene.

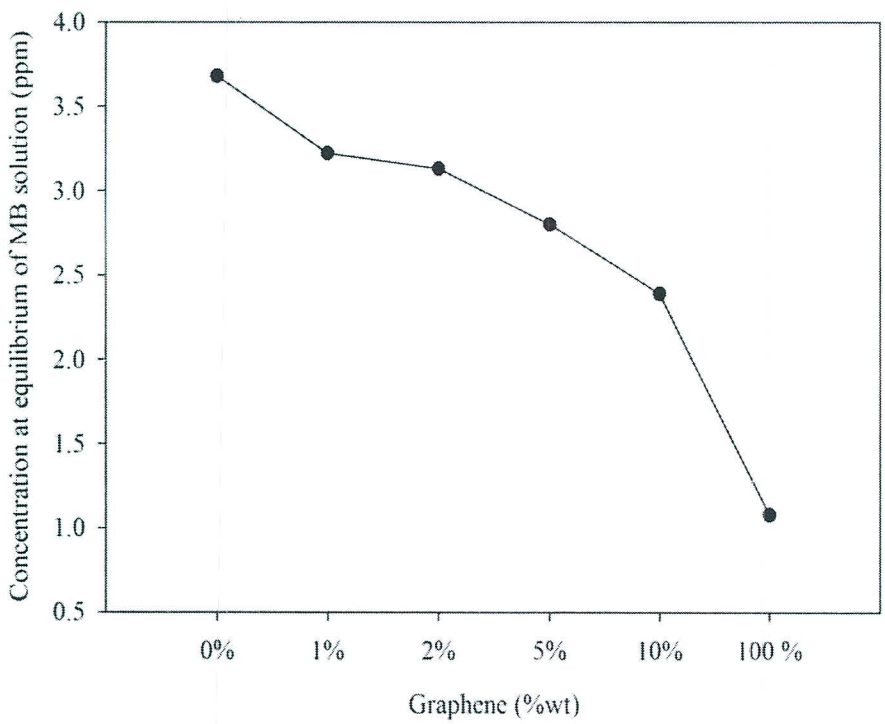

Figure 4.10 Concentration at equilibrium of MB solution (ppm) in the presence of TiO_2, GR–TiO_2 (PTA) and graphene.

The photocatalytic activities of the GR–TiO_2 (PTA) series of experiments under UV and visible light irradiation are presented in Figures 4.11 and 4.12, respectively. In GR–TiO_2 (PTA) series, the order is GR–TiO_2 (PTA, 1:50) > GR–TiO_2 (PTA, 1:20) > GR–TiO_2 (PTA, 1: 10) > GR–TiO_2 (PTA, 1:100) > TiO_2 (PTA) > P25. The optimal amount of graphene seems to be within the range of 1:10 to 1:100 because the photocatalytic activities of GR–TiO_2 (PTA) at 1:10 and 1:100 become close to those of pure TiO_2 (PTA). The appropriate amount of graphene to TiO_2 for preparation GR–TiO_2 (PTA) in this experiment is about 1:50. The decrease in MB degradation efficiencies of GR–TiO_2 (PTA, 1:10 and 1:20) under UV and visible light compared to that of GR–TiO_2 (PTA, 1:50) was ascribed to light obstruction. In Figure 4.7, GR–TiO_2 (PTA, 1:10 and 1:20) yields higher absorption over all visible light wavelengths. In Figure 4.9, the photocurrent generations of GR–TiO_2 (PTA, 1:10 and 1:20) photocatalyst under UV and visible light irradiation are lower than that of GR–TiO_2 (PTA, 1:50). These evidences imply that the overdose graphene content in GR–TiO_2 reduces the absorption efficiency of light by TiO_2 (Zhang et al., 2012).

The photoexcitation process needs sufficient energy from the photons to excite the electrons in the valance band to the conduction band of TiO_2. Graphene has black color, consists in π–π conjugated system that can absorb wide range of photon energy. Therefore, the excessive of graphene in GR–TiO_2 acting as a detrimental photon absorption material leads to decrease in photocurrent generation and degradation efficiency of photocatalyst. The concentration at equilibrium of MB solution in the presence of GR–TiO_2 (PTA) photocatalysts at different weight ratio of graphene was compared with pure TiO_2 (PTA) and graphene as shown in Figure 4.10. In the dark condition, the MB molecules adsorbed onto catalysts and reached equilibrium in dark condition within 3 h.

The remaining concentration of MB in the presence of GR–TiO_2 composites is lower than that of TiO_2. The BET specific area of TiO_2 (PTA), GR–TiO_2 (1:100), GR–TiO_2 (1:50), GR–TiO_2 (1:20) and GR–TiO_2 (1:100) was presented in Table 4.2. It was obvious that the BET specific area of GR–TiO_2 (PTA) increases with increasing weight ratio of graphene resulting in an increase in adsorbability.

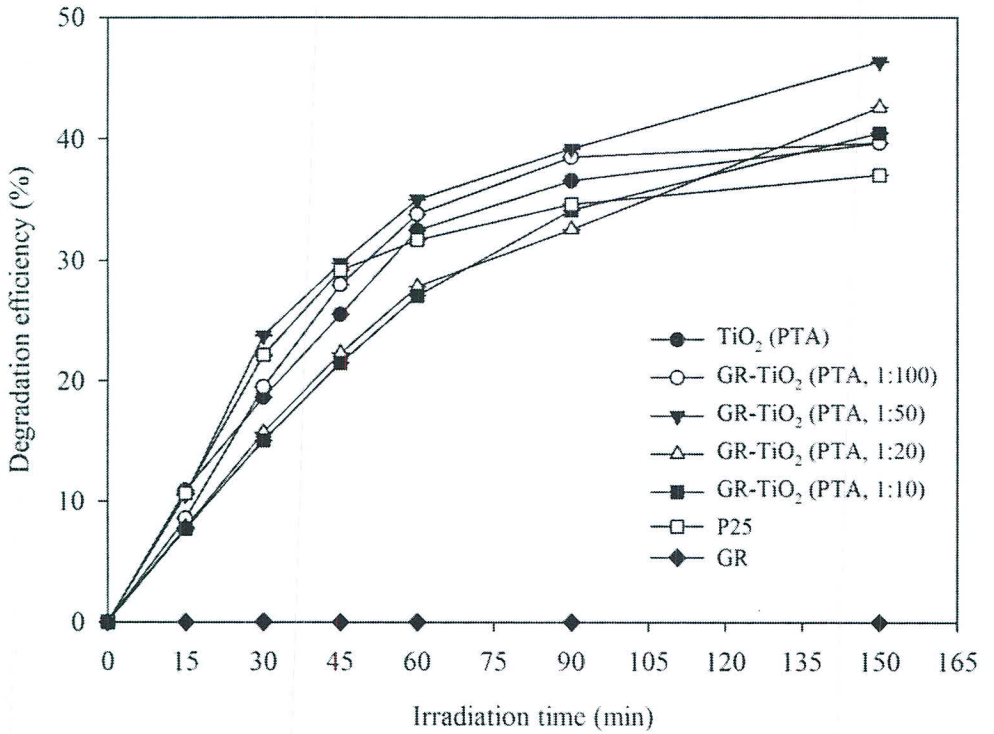

Figure 4.11 Degradation efficiency of photocatalysts under UV irradiation.

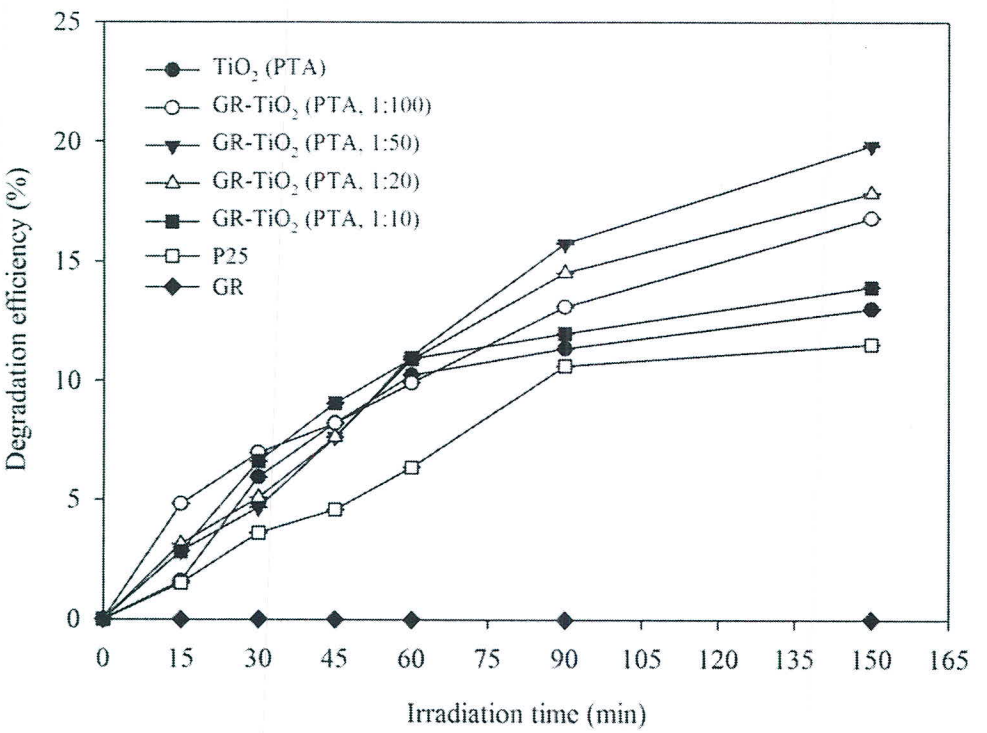

Figure 4.12 Degradation efficiency of photocatalysts under visible light irradiation.

In this study, the photodegradation of MB in the presence of P25 photocatalyst under UV and visible light irradiation is not as high as that of TiO_2 (PTA). The average crystal size of P25 calculated using Scherrer's equation is about 21.1 nm and it was also observed that P25 has the lower BET specific area (50.75 $m^2 g^{-1}$) than that of TiO_2 (PTA, 88.00 $m^2 g^{-1}$). Therefore, the decrease in photocatalytic activity of P25 is due to its lower specific surface area.

The possible mechanism for enhanced adsorbability on GR–TiO_2 (PTA) should be a noncovalent formation which is formed on the surface of graphene via the interaction between the π–π stacking of MB molecules and aromatic regions of graphene (Zhang et al., 2011). It has been reported that 17β-estradiol molecules were trapped on graphene pores and further degraded by Fe doped TiO_2 (Farhangi et al., 2011). Thus, the MB molecules, also adsorbed, trapped and then degraded by TiO_2 photocatalyst. The photocatalytic activity of GR–TiO_2 (PTA) under visible light irradiation was influenced by narrowing of the band gap from 3.24 to 2.90, which resulted in the formation of Ti–O–C bonds according to the FTIR spectra (Figure 4.3). The GR–TiO_2 (PTA, 1:50) catalyst showed higher photocatalytic activity than any other catalyst. However, in the case of GR–TiO_2 (PTA, 1:20) and GR–TiO_2 (PTA, 1:10) the BET surface areas are 102.00 and 105.70 $m^2 g^{-1}$, respectively. Both catalysts show larger surfaces than that of GR–TiO_2 (PTA, 1:50) but their photocatalytic activities are not as high as that of GR–TiO_2 (PTA, 1:50). Therefore, the addition of higher graphene content in a GR–TiO_2 (PTA) photocatalyst not only leads to a decrease in photocatalytic activity because of light obstruction but also shields the active sites on TiO_2 photocatalyst (Cheng et al., 2012).

The degradation efficiency of GR–TiO_2 under UV and visible light irradiation is around 35–90% and 10–65%, respectively. The difference in the quantity of degradation efficiency is generally attributed to three main factors: the power of the light source (300–500 W Xe lamp or 100 W high pressure Hg lamp), the amount of photocatalyst mass in the reactor (0.01–0.05 g L^{-1}) and dye (methylene blue, methyl orange and rhodamine B (indicator for determination of the photocatalytic activity of photocatalyst)). However, in this research work, UV (8 W BLB lamp) or fluorescent lamp (8 W fluorescent lamp) was used and the photocatalyst that was loaded in reactor was about 1.0 mg. Thus, the

degradation efficiency of photocatalyst may be lower than that report in others studies (Wang and Zhang, 2011c and Zhang et al., 2010a).

Theoretically, it is well known that the electrons in the valence band (VB) can be excited to the conduction band (CB) of TiO_2 by photo–irradiation. This reaction leads to positive holes in the VB and electrons in the CB that can further react with adsorbed water and oxygen molecules to produce hydroxyl radicals ($^{\bullet}OH$) and superoxide radical anions ($^{\bullet}O_2^-$) which can oxidize volatile organic compounds(Tseng et al., 2010). The formation of $^{\bullet}OH$ and $^{\bullet}O_2^-$ in the presence of TiO_2 photocatalyst is well known and written as shown in Equations (4.1)–(4.5) (Houas et al., 2001 and Kaewitp et al., 2012b).

$$TiO_2 + h\nu \longrightarrow TiO_2\,(h^+) + TiO_2\,(e^-) \quad (4.1)$$

$$O_2 + e^- \longrightarrow {}^{\bullet}O_2^- \quad (4.2)$$

$$2{}^{\bullet}O_2^- + 2H_2O \longrightarrow 2H_2O_2 + O_2 \quad (4.3)$$

$$H_2O_2 + e^- \longrightarrow {}^{\bullet}OH + OH^- \quad (4.4)$$

$$h^+ + Ti\text{–}OH^- \longrightarrow Ti\text{–}{}^{\bullet}OH \quad (4.5)$$

The photocatalytic activity of GR–TiO_2 (PTA) composite is improved by the separation of the photo-generated electrons and holes. Graphene acts as electron acceptor and transporter due to its π–π conjugation structure (Khalid et al., 2012 and Farhangi et al., 2011) and high conductivity (Hou et al., 2012). The TiO_2 electrons from the VB can be excited to the CB, and then rapidly transfer to graphene, leaving more electron–hole pairs to produce highly reactive species ($^{\bullet}OH$ and $^{\bullet}O_2^-$), resulting in higher photocatalytic activity.

4.3 Conclusions

The GR–TiO_2 photocatalysts were synthesized via PTA as a precursor with different weight ratios of graphene. GR–TiO_2 (PTA) contains anatase phase crystal with an average length of 80–90 nm and diameter of 20–22 nm. The surface area of GR–TiO_2 (PTA) photocatalyst increased with increasing weight ratio of graphene. Under UV and visible light irradiation, GR–TiO_2 (PTA, 1:50) photocatalyst has the optimal amount of added graphene to achieve the highest photocatalytic activity, while a higher or lower weight ratio of graphene content seems to decrease the photocatalytic activity. The enhancement of photocatalytic activity can be attributed to the influence of the increase in adsorption

capacity of graphene and the reduction of the band gap by the formation of Ti–O–C bonds. The charge recombination process of electron–hole pairs can be suppressed because the π–π conjugated system of graphene provides good a electron acceptor.